

Simulations of CFC content and water mass age in the deep North Atlantic

Matthew H. England¹

Centre for Environmental Modelling and Prediction, School of Mathematics, University of New South Wales, New South Wales, Australia

Greg Holloway

Institute of Ocean Sciences, Sidney, British Columbia, Canada

Abstract. A series of numerical model experiments are studied with a view to determine whether the chlorofluorocarbon (CFC) burden in the North Atlantic Deep Western Boundary Current (DWBC) can be simulated realistically in models of coarse horizontal resolution. Five main model cases are considered, covering three different parameterizations of subgrid-scale mixing (standard Cartesian, isopycnal, and the eddy advection scheme of *Gent et al.* [1995]), a version with enhanced surface thermohaline forcing, and, finally, a case that incorporates the effects of topographic stress as in *Alvarez et al.* [1994]. Most model experiments exhibit deficient CFC content in the DWBC, except, notably, the case with a tightly constrained wintertime thermohaline forcing in the North Atlantic, as well as the run which includes the effects of topographic stress. However, the approach of strongly restoring surface temperature-salinity to observations yields excessive heat loss and large freshwater fluxes during winter and so cannot be recommended as a technique to rectify deficient North Atlantic Deep Water production in ocean models. Overall, the coarse-resolution simulations only resolve a relatively weak and diffuse CFC signal in the DWBC in the North Atlantic and typically only capture one CFC-bearing core. This is primarily due to model currents in the deep North Atlantic being too slow and broad compared to the real ocean, as well as a spurious tendency for the outflow to recirculate and upwell into the Gulf Stream. The model runs do not capture a deeper CFC core because they all fail to simulate a dense water overflow off the Greenland-Iceland-Scotland Ridge. Seawater age is analysed in each of the experiments using an idealized age tracer as well as the simulated CFC-11/CFC-12 ratio. The CFC ratio estimates water in the DWBC at the equator to be between 25 and 33 years old. In contrast, the equilibrated age tracer ranges from 141 to 210 years. The CFC-estimated age is substantially younger than the true seawater age because of a mixing bias when CFC-free waters are entrained into the DWBC. This is possible because old CFC-free waters cannot alter the CFC-11/CFC-12 ratio of CFC-burdened water, even though the true age is affected by such a dilution. It is therefore suggested that caution be taken when adopting the CFC-11/CFC-12 ratio to extrapolate seawater age in waters where significant dilution with CFC-free waters has occurred.

1. Introduction

The Deep Western Boundary Current (DWBC) in the North Atlantic Ocean is a key component of the global thermohaline circulation. It transports a substantial amount of North Atlantic Deep Water (NADW) across the equator and into the Southern Ocean (12–15 Sv) ($1 \text{ Sv} = 10^6 \text{ m}^3 \text{ s}^{-1}$) [*Schmitz, 1995*], forming an important limb of the ocean's global conveyor belt [*Broecker, 1991*]. By mass conservation the DWBC must be balanced by an upper ocean flow into the far North Atlantic to replace the exported NADW, which affects the net meridional heat and freshwater transports in the North Atlantic and climate in the northern hemisphere.

The strength of overturning in the North Atlantic has been the subject of a number of modeling studies in recent years. In studies of the sensitivity of NADW production rates to basic model configuration, researchers have found the NADW overturn to be determined by many factors, including model resolution [*Böning et al., 1996*], mixing parameterization [*Bryan, 1987; England, 1995a; Böning et al., 1995; Robitaille and Weaver, 1995*], thermohaline forcing in the North Atlantic [*England, 1993; Döscher et al., 1994*], and the strength of the westerly wind belt in the Southern Ocean [*Toggweiler and Samuels, 1992*]. In the present study we will monitor the strength of the DWBC in the North Atlantic and its simulated chlorofluorocarbon (CFC) burden in several configurations of a commonly used ocean general circulation model.

The use of CFCs as a tracer of the model ocean circulation is particularly important in the context of simulating the DWBC. Conventional hydrographic tracers such as temperature and salinity offer only limited information on the accuracy of the model DWBC, giving a qualitative measure of how realistically the model exports relatively warm and saline

¹Also affiliated with Division of Atmospheric Research, CSIRO, Aspendale, Victoria Australia.

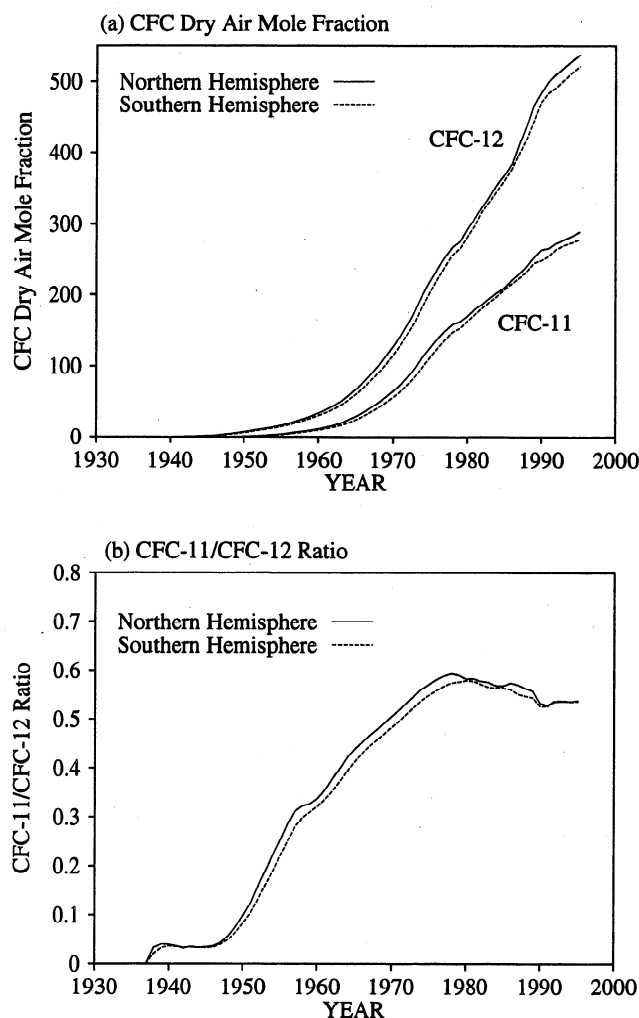


Figure 1. Reconstructed history of (a) the atmospheric dry air mole fractions of CFC-11 and CFC-12 and (b) their ratio (CFC-11/CFC-12). The solid lines correspond with estimates for the northern hemisphere, and dashed lines for estimates in the southern hemisphere. In effect, the southern hemisphere concentrations lag the northern hemisphere values by just over 1 year.

NADW into the Southern Ocean. In contrast, because CFCs are transient tracers (Figure 1), they can tell us whether the model DWBC is rapid enough compared to the real ocean, whether the current itself is too broad or narrow, and whether it follows the observed outflow path. These are more stringent tests on the ocean simulation than simply checking the production rate of NADW, particularly when the model NADW that is overturned may never reach the Southern Ocean (because of spurious circulation patterns in the DWBC).

Substantial measuring of CFC content in the North Atlantic has been performed in recent years, for example, as part of the Transient Tracers in the Ocean (TTO) North and Tropical Atlantic Studies [Weiss *et al.*, 1985] and within the Western Boundary Exchange Experiment (WBEX) [Smethie, 1993]. These CFC data dramatically reveal the pathway of transport of the DWBC (refer, for example, to Figures 3a, 4a, and 7a) and have been used to quantify the speed and pathway of deep currents in the North Atlantic [e.g., Weiss *et al.*, 1985; Pickart *et al.*, 1989; Smethie, 1993; Rhein, 1994]. Weiss *et*

al. [1985] identify a well-defined core of relatively high CFC concentration water near 1600-m depth at the equator in Upper NADW during early 1983 (see Figure 4a). Farther upstream in the outflowing NADW (32°–45°N), Smethie [1993] finds two distinct layers of CFC near the continental slope, one in Upper NADW near 800- to 1500-m depth and one in Lower NADW at about 3500-m depth, the shallower maximum having higher CFC content at a given latitude (e.g., Figure 7a). The deeper core originates from dense water with classical NADW properties overflowing the Greenland-Iceland-Scotland Ridge [Smethie, 1993], a feature not typically resolved by coarse-resolution ocean models [e.g., Toggweiler *et al.*, 1989; England, 1993; Hirst and Cai, 1994].

In this paper we present results from a set of numerical experiments designed to assess the sensitivity of the DWBC to changes in model physics or forcing which are known to affect the deep water outflow in the North Atlantic. By directly modeling the CFC burden in the outflow current we will be able to determine which ocean model configuration yields improved representation of transient ocean ventilation in the DWBC over the decadal to interdecadal timescale. In addition, an idealized age tracer and the model-simulated CFC-11/CFC-12 ratio are used to study the rate of seawater renewal in the DWBC in the model cases. It will be shown that substantially different renewal rates are simulated in the DWBC, depending on the model ocean forcing and mixing parameterizations adopted.

The rest of this paper is divided into five sections. In section 2 we describe the ocean model and experimental design adopted for the present study. The method used for modeling CFC exchange across the air-sea interface is summarized in section 3 along with a definition of the model equilibrated seawater age. Section 4 covers the analysis of the CFC burden in the DWBC in each case, and then, in section 5, the seawater age and renewal timescales are examined. Finally, section 6 covers the concluding remarks.

2. Ocean Model and Experimental Design

The ocean model used in this study is the Bryan-Cox ocean GCM developed at the Geophysical Fluid Dynamics Laboratory (GFDL) [Bryan, 1969; Cox, 1984; Pacanowski *et al.*, 1991]. Five main versions of the model are considered, each with identical geometry, though with differing treatment of subgrid-scale mixing and surface thermohaline forcing. The configuration of the “control” case is very similar to that used by England *et al.* [1994] and England [1995b], and so only a brief overview is presented here. The model domain has a global coverage of the world ocean extending from the Antarctic continent to the north pole, with a realistic representation of the ocean bottom bathymetry. The model grid spacing is 3.75° longitude by ~4.5° latitude with 12 unequally spaced vertical levels. The effects of mesoscale processes are taken into account implicitly by parameterizations of subgrid-scale mixing of momentum and tracers. The horizontal (A_{MH}) and vertical (A_{MV}) viscosity coefficients are taken to be constants independent of depth ($A_{MH} = 2.5 \times 10^9 \text{ cm}^2 \text{ s}^{-1}$; $A_{MV} = 50 \text{ cm}^2 \text{ s}^{-1}$). Model tracers (potential temperature (T), salinity (S), CFC-11, CFC-12, and idealized age) are subject to diffusion as detailed in Tables 1 and 2, as well as to advection and vertical convection. Vertical diffusion (A_{HV}) is lowest in the surface layer ($0.3 \text{ cm}^2 \text{ s}^{-1}$), increasing below the thermocline toward a maximum of $1.3 \text{ cm}^2 \text{ s}^{-1}$ in the deeper model levels. The hori-

Table 1. Experimental Design Adopted for the Present Study

Experiment	Integration Time, years	Surface Forcing	Subsurface Mixing
CTRL	4750	seasonal climatology	horizontal mixing, A_{HH}
ISOP	3650	seasonal climatology	isopycnal mixing, background A_{HH}
GM	5850	seasonal climatology	<i>Gent and McWilliams</i> [1990], $A_{HH} = 0$
NAW	4200	strong winter restoring in NA	horizontal mixing, A_{HH}
TOPO	3600	seasonal climatology	horizontal mixing, topographic stress

Each model experiment is integrated until equilibration without using vertical acceleration techniques. The transient CFC simulations are then conducted over much shorter periods (around 65 years), corresponding with an integration nominally during 1930–1995. A_{HH} is the horizontal diffusion coefficient, and NA denotes the North Atlantic Ocean and associated seas north of 45°N. The five cases listed are the control (CTRL), isopycnal mixing (ISOP), *Gent and McWilliams* [1990] (GM), North Atlantic winter (NAW), and topographic stress (TOPO) experiments.

zonal diffusivity (A_{HH}) varies between experiments as described below. Convection is treated implicitly by the model; whenever gravitational instabilities in stratification are detected, the vertical diffusion rate is increased to simulate com-

plete mixing over the unstable portions of the water column. This vertical mixing homogenizes all tracers over the model levels originally detected to be dynamically unstable. No parameterization is included for deepening the surface mixed layer by wind-driven turbulence; that is, the convection of vertically unstable waters remains the only way deep mixed layers are formed in the model.

The ocean is forced at the sea surface by seasonally varying climatological boundary conditions of temperature, salinity, and wind stress. The atmosphere to ocean momentum flux is determined from the wind stress climatology of *Hellerman and Rosenstein* [1983] interpolated spatially onto the model grid and temporally at each time step. The effective surface fluxes of heat and freshwater are implied by restoring the model's surface layer temperature and salinity toward the *Levitus* [1982] seasonal climatology. Surface T - S are restored using a Newtonian timescale of $(30 \text{ days})^{-1}$ for T and $(50 \text{ days})^{-1}$ for S . Apart from including a seasonal cycle in the sea surface conditions, the control case carries none of the boundary condition embellishments available for improved T - S representation [see, e.g., *England*, 1993]. In all experiments considered, the ocean model is integrated with a fixed T - S time step of 30 hours at all depths. The integrations continue until the equilibrium criterion of *England* [1993] is met, which in all cases requires 3000 to 4000 model years (Table 1).

The five principal experiments are as listed in Table 1. The control experiment (CTRL) was used to examine the sensitivity of the CFC simulation to a range of air-sea gas exchange parameterizations in work by *England et al.* [1994]. It adopts traditional Cartesian mixing with a horizontal diffusivity A_{HH} which decreases with depth ($A_{HH} = 1 \times 10^7 \text{ cm}^2 \text{ s}^{-1}$ in the surface level decreasing gradually toward $0.5 \times 10^7 \text{ cm}^2 \text{ s}^{-1}$ at depth; after *Bryan and Lewis* [1979] and *Toggweiler et al.* [1989]).

The next two experiments feature introduction of parameterizations for the effect of mesoscale eddies. In the second experiment, "isopycnal mixing" (ISOP), the widely used scheme of *Redi* [1982] and M.D. Cox (unpublished manuscript, 1987) is adopted to include the effect of tracer diffusion along isopycnal surfaces. This scheme has been shown to have only a small effect on the deep water density field [*England*, 1993; *Hirst and Cai*, 1994], but is included here because it permits additional pathways for penetration of CFC into the ocean interior (by diffusion along the isopycnal surfaces). It differs from the Control case only in that the mixing of tracers is enhanced along the isopycnal surfaces, and the horizontal diffusivity is changed to a constant background value of $A_{HH} = 0.75 \times 10^7 \text{ cm}^2 \text{ s}^{-1}$. The isopycnal

Table 2. Vertical Grid Spacing and the Vertical, Horizontal, and Isopycnal Mixing Coefficients Used in the Model Runs

Level	ΔZ	Z	A_{HV}	A_{HH}	A_p
1	50.9	50.9	0.305	0.98×10^7	4.80×10^7
2	68.4	119.3	0.306	0.92×10^7	4.37×10^7
3	100.4	219.7	0.307	0.86×10^7	3.85×10^7
4	151.1	370.8	0.310	0.78×10^7	3.22×10^7
5	224.0	594.8	0.314	0.69×10^7	2.52×10^7
6	319.6	914.4	0.321	0.61×10^7	1.88×10^7
7	432.5	1346.9	0.339	0.55×10^7	1.42×10^7
8	551.0	1897.9	0.393	0.52×10^7	1.16×10^7
9	660.9	2558.8	0.887	0.51×10^7	1.05×10^7
10	751.9	3310.7	1.236	0.50×10^7	1.01×10^7
11	820.4	4131.1	1.280	0.50×10^7	1.00×10^7
12	868.9	5000.0	1.300	0.50×10^7	1.00×10^7
1	50.9	50.9	0.305	0.98×10^7	4.80×10^7
2	61.4	112.3	0.306	0.92×10^7	4.40×10^7
3	73.6	185.9	0.307	0.87×10^7	3.97×10^7
4	85.9	271.8	0.308	0.82×10^7	3.53×10^7
5	99.0	370.8	0.310	0.76×10^7	3.10×10^7
6	107.5	478.3	0.312	0.71×10^7	2.71×10^7
7	116.5	594.8	0.314	0.67×10^7	2.37×10^7
8	143.8	738.6	0.317	0.63×10^7	2.05×10^7
9	175.8	914.4	0.322	0.60×10^7	1.77×10^7
10	194.6	1109.0	0.328	0.57×10^7	1.53×10^7
11	237.9	1346.9	0.339	0.54×10^7	1.34×10^7
12	263.0	1609.9	0.357	0.53×10^7	1.21×10^7
13	288.0	1897.9	0.393	0.52×10^7	1.12×10^7
14	317.2	2215.1	0.496	0.51×10^7	1.07×10^7
15	343.7	2558.8	0.886	0.51×10^7	1.03×10^7
16	360.9	2919.7	1.162	0.50×10^7	1.02×10^7
17	391.0	3310.7	1.236	0.50×10^7	1.01×10^7
18	404.0	3714.7	1.264	0.50×10^7	1.00×10^7
19	416.4	4131.1	1.280	0.50×10^7	1.00×10^7
20	425.8	4555.9	1.289	0.50×10^7	1.00×10^7
21	444.1	5000.0	1.295	0.50×10^7	1.00×10^7

Grid box thickness (ΔZ) and depth of the base of each model level (Z) are shown for both the 12- and 21-level cases. Also shown are values of the vertical (A_{HV}), horizontal (A_{HH}), and isopycnal (A_p) diffusivities adopted. Tracer mixing parameters are fixed in experiments CTRL, NAW, and TOPO (with $A_p = 0$). In ISOP, A_p is nonzero (taking values as shown above), and A_{HH} is constant ($0.75 \times 10^7 \text{ cm}^2 \text{ s}^{-1}$). In experiment GM, A_{HH} is zero everywhere, and the extra mixing term of *Gent et al.* [1995] is included (with $\kappa = 1 \times 10^7 \text{ cm}^2 \text{ s}^{-1}$).

diffusion decreases with depth between surface and deep values ($5.0 \times 10^7 \text{ cm}^2 \text{ s}^{-1}$ in the surface layer gradually decreasing to $1.0 \times 10^7 \text{ cm}^2 \text{ s}^{-1}$ at depth, Table 2). The choice of isopycnal and horizontal diffusivity in experiment ISOP is therefore exactly as in *Manabe et al.* [1991, 1992].

In the third experiment, "GM", we include the scheme of *Gent and McWilliams* [1990] and *Gent et al.* [1995] for representing adiabatic transport effects of baroclinic eddies. The results of *Danabasoglu et al.* [1994], *England* [1995a], *Danabasoglu and McWilliams* [1995], and *Hirst and McDougall* [1996] demonstrate that use of this scheme results in marked increases in the deep water density and an associated reduction in convection. They also indicate improvements in the steady state simulation of deep temperature and salinity, although the sensitivity of transient ventilation rates in the DWBC to the scheme remains largely unexplored.

The GM experiment differs from ISOP in that (1) a parameterization is included for the effect of eddy-induced transport as per *Gent et al.* [1995], (2) the horizontal diffusivity is set to zero, and (3) the number of model levels is increased to 21. This increase in vertical resolution is required to achieve the level of numerical stability found necessary to run the GM case without horizontal diffusivity. The model levels for the GM experiment are listed in Table 2 and are chosen in such a way as to ensure that no changes to the model topography were necessary (since all model bathymetric features are at least 370.8 m deep). The ISOP and CTRL experiments were also rerun with the 21 levels used in GM, with little change in results for CFC uptake and overall model ventilation rates. This is discussed further in the appendix.

The implementation of the *Gent et al.* [1995] parameterization is as detailed by *Hirst and McDougall* [1996]. The "isopycnal thickness diffusivity" κ , which determines the strength of the eddy-induced transports, is set at $1.0 \times 10^7 \text{ cm}^2 \text{ s}^{-1}$ [after *Danabasoglu et al.*, 1994; *Hirst and McDougall*, 1996]. This value is supported by the analysis of *Rix and Willebrand* [1996] of an eddy-resolving Atlantic model with $1/3^\circ$ horizontal resolution. They perform their analysis of the GM thickness diffusion term for a region of the North Atlantic ($10^\circ\text{--}30^\circ\text{N}$, $20^\circ\text{--}60^\circ\text{W}$). On the other hand, *Visbeck et al.* [1997] present strong arguments that the value of κ should depend on the local vertical and horizontal stratification and should vary by an order of magnitude or so between different regions of the ocean. They use idealized experiments to estimate that κ should be $2.0 \times 10^7 \text{ cm}^2 \text{ s}^{-1}$ in a wind-driven channel resembling the Antarctic Circumpolar Current but only $0.3 \times 10^7 \text{ cm}^2 \text{ s}^{-1}$ in a typical convection region. Model experiments adopting a spatially varying value for κ should be explored in future studies.

A highly desirable feature of the *Gent et al.* [1995] parameterization is that it allows the model to be run with small or zero horizontal diffusivity. There is little physical justification for inclusion of horizontal diffusivity [e.g., *McDougall and Church*, 1986], and it is retained in the other experiments solely to ensure numerical stability. It has been shown to significantly degrade model solutions, for example, by facilitating unrealistically large diapycnal flux of buoyancy and by inducing large diapycnal volume transports [e.g., *Veronis*, 1975; *England*, 1993; *Böning et al.*, 1995; *Hirst et al.*, 1996].

In the fourth experiment we alter the surface thermohaline forcing in the North Atlantic Ocean during the northern hemi-

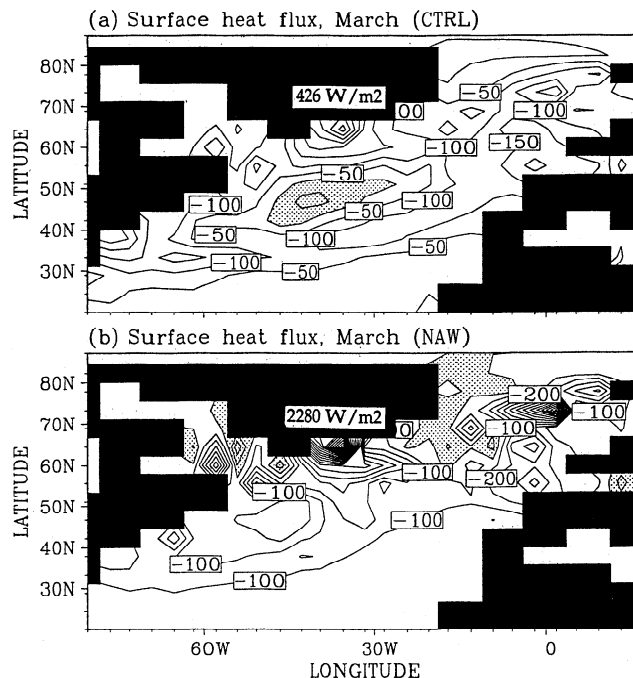


Figure 2. Diagnosed mean surface heat fluxes during March (in W m^{-2}) in experiments (a) control (CTRL) and (b) North Atlantic winter (NAW) over the northern North Atlantic. Stippled regions denote a surface heat gain during March.

sphere winter. This experiment is called the "North Atlantic winter" experiment (NAW); it differs from the control experiment only in that the restoring coefficient for both T and S is reduced to $(5 \text{ days})^{-1}$ in the Atlantic Ocean and associated seas north of 45°N during three wintertime months. While the shorter restoring time scale ensures realistic surface T - S conditions in the North Atlantic during winter, it also leads to unrealistic heat and freshwater fluxes in certain locations (Figure 2). For example, maximum wintertime surface heat loss southeast of Greenland increases from 426 W m^{-2} (CTRL) to 2280 W m^{-2} (NAW) compared with an observed climatological maximum of around 260 W m^{-2} [*Esbenson and Kushnir*, 1981]. Other regions of spurious winter ocean heat loss appear in the Norwegian Sea (e.g., 1340 W m^{-2} near 0° , 73°N). The strong restoring toward observed T - S is therefore a way of correcting the model water mass properties by imposing large surface fluxes that compensate for otherwise unrealistic model behavior. The surface waters in experiment NAW become realistically cold, saline, and dense because of the strong Newtonian restoring. For example, peak surface density (σ_θ) in the Greenland-Norwegian Sea increases from 27.74 kg m^{-3} in CTRL to 27.98 kg m^{-3} in experiment NAW, which is much closer to the peak value of 27.97 kg m^{-3} implied from the *Levitus* [1982] climatology.

In the final model experiment (TOPO) the parameterization of topographic stress of *Alvarez et al.* [1994] and *Eby and Holloway* [1994] is incorporated into the model momentum equations (through the eddy viscosity terms). This implies that the model ocean currents relax toward a state of maximum entropy that depends on the shape of the subsurface topography. In the other four experiments, in contrast, the ocean velocity field would relax toward a state of rest. *Eby and Holloway* [1994] have shown that this parameterization of the

effects of eddies interacting with topography leads to a model solution with an intensified DWBC, as well as generating poleward Deep Eastern Boundary Currents. This can be expected to substantially change the CFC burden in the outflow currents in the North Atlantic.

3. Simulating CFC Uptake and Seawater Age in the Model

3.1. Including CFC Uptake

To run a simulation of CFC uptake, the equilibrated ocean model is restarted with two additional tracers (CFC-11 and CFC-12) initially at zero concentration everywhere. The model is then run nominally from year 1930 until the end of 1995 with an ocean uptake of CFC-11 and CFC-12 (whose atmospheric histories are shown in Figure 1). The forcing of CFC fluxes in the present study follows the most realistic case presented by *England et al.* [1994], as detailed more recently by *England and Hirst* [1997]. The parameterized uptake of CFC-11 and CFC-12 follows the physical law governing air-sea gas exchange, namely

$$Q = k(\alpha C_{\text{atm}} - C_w) \quad (1)$$

where Q is the gas flux across the air-sea interface (fluxes from the atmosphere into the ocean are positive), k is the gas transfer speed, α is the solubility coefficient of the given gas (taken from *Warner and Weiss* [1985]), C_{atm} is the atmospheric concentration over the sea surface, and C_w is the concentration of CFC in the near-surface seawater. In the present series of experiments, k is parameterized following *Wanninkhof* [1992] with an additional sea ice factor, namely

$$k = k_0 u^2 [1 - R] / \sqrt{Sc} \quad (2)$$

where k_0 is a constant (7.964) derived from bomb-produced radiocarbon invasion rates into the ocean (which includes implicitly the Schmidt number for ^{14}C), u is the climatological wind speed (in m s^{-1}), R is the fraction of sea ice cover (derived from *Parkinson et al.* [1987] and *Comiso et al.* [1993]), and Sc is the Schmidt number for the given gas. In the calculation of k we reference the *Esbenson and Kushnir* [1981] seasonally varying wind speeds and compute Sc as a function of climatological temperature for each gas. That is, k varies seasonally on account of seasonal changes in the surface wind speed, sea ice cover, and upper level temperature (through its determination of the Schmidt number Sc).

To compute the T - S dependent solubility (α) of CFC-11 and CFC-12, we reference the observed seasonal T - S climatology (not the model-predicted T - S). This is done to ensure that all model experiments have the same reference saturation levels of CFC-11 and CFC-12. Actual surface level concentrations will then vary according to differences in simulated convection and vertical motions. Differences in surface level T - S between the cases will therefore not directly affect the upper level CFC concentration through the solubility term, only indirectly through its influence on convection and vertical motion patterns.

In work by *England et al.* [1994] it was shown that a wind speed dependent parameterization of surface CFC exchange reproduced many of the subtle variations in upper ocean saturation levels, namely, undersaturation in regions of deep con-

vective overturn and near-surface upwelling, and supersaturation in the summer mixed layer. In addition, the sea ice factor is necessary to limit the air-sea gas transfer in direct proportion to the observed seasonally varying sea ice coverage.

In summary, a controlled surface forcing has been adopted as in the study of *England and Hirst* [1997] to minimize the uncertainties in analyzing the different CFC simulations. This includes using identical (though temporally and spatially varying) solubility distributions, wind speeds, sea ice cover, and Schmidt numbers in each of the experiments. Variations in the CFC simulations then result only as a function of differing vertical convection, overturn, and circulation between the respective model cases.

3.2. Modeling Seawater Age

Two estimates of model seawater age will be examined in this paper. One is based on an idealized age tracer that is defined as the volume-weighted time scale for surface waters to communicate with the ocean interior (described later). The other is based on the simulated CFC-11/CFC-12 ratio in each model case. Before the discovery that chlorofluorocarbons act to deplete the Earth's ozone layer [*Molina and Rowland*, 1974] the CFC-11/CFC-12 ratio increased steadily with time (Figure 1b). This property can be used to estimate the age of subsurface waters in both ocean measurements [e.g., *Gammon et al.*, 1982; *Weiss et al.*, 1985] and in our model simulations. Because the CFC-11/CFC-12 ratio has remained approximately constant (near 0.57) since 1975, we can only use this technique to estimate the age of water exposed to the atmosphere before this time. In addition, significant atmospheric traces of CFC-11 do not appear until the early 1950s, so we can at best trace water parcels that are around 45 years old. Since our interest is focused on the DWBC, when calculating ages, we consider the CFC distributions during the same simulation year as those used in our analysis of the CFC-11 content in the DWBC (i.e., 1983). This gives the deep water mass traces of CFC-11 and CFC-12 a reasonable time to ventilate the ocean interior in the North Atlantic. For water with a CFC-11/CFC-12 ratio >0.54 we can only give an upper age limit of 10 years.

The CFC ratio estimate of age suffers from a bias toward younger age when CFC-free waters contaminate the water sample in question. For example, suppose that a water sample measured in the DWBC is comprised of one-third recently formed Labrador Sea Water (LSW), with CFC concentrations c_{11} and c_{12} at formation time, and two-thirds waters that are CFC free. The CFC-free water might originate from recirculations in the North Atlantic or older upwelled Weddell Sea Bottom Water. For the purpose of this example we will suppose the LSW to be 20 years old and the CFC-free water to be 200 years old, noting that the CFC-free mixture is likely to comprise source waters that are even older. On dilution the original CFC-11/CFC-12 ratio (c_{11}/c_{12}) would remain unchanged, since the dilution process weakens the CFC-11 and CFC-12 concentrations in the same proportion. So the water mass mixture would appear to be only 20 years old (with CFC-11/CFC-12 ratio identical to its original LSW component), even though its true age is $[(200 \times 2) + (20 \times 1)]/3 = 140$ years old. The CFC estimate of age should therefore be considered an approximate measure of the age of water in the DWBC that was in contact with the atmosphere since the late 1950s and not the true equilibrated age of the water mass mixture.

To convert the CFC-11/CFC-12 ratio of a given water sample into an atmospheric CFC ratio requires some knowledge of the surface T - S properties at the time when the water parcel was exposed to the atmosphere. This is because we need to divide the ocean concentrations by the CFC solubilities to obtain the original atmospheric conditions (and therefore be able to date the water mass using the data in Figure 1b). Errors in estimating the original T - S properties of the water mass do not introduce large errors into the age estimate, particularly for salinity. For example, the CFC solubility ratio is nearly identical for water of $(T, S) = (0^\circ\text{C}, 34.0\text{‰})$ and water of $(T, S) = (0^\circ\text{C}, 35.0\text{‰})$ at 4.1001 and 4.0997, respectively. Even a 3°C change in T does not greatly change the solubility ratio (e.g., water of $(T, S) = (3^\circ\text{C}, 35.0\text{‰})$ has a solubility ratio of 4.0099). For the purposes of our model CFC ratio estimates of age we assume that the source waters in the DWBC are predominantly LSW formed in the winter mixed layer (with T - S properties 3.5°C and 34.9‰). The possible errors introduced by such an assumption are very small compared with those caused by the dilution of the DWBC by waters that are CFC free.

A more rigorous diagnosis of model water age can be obtained by configuring an additional numerical tracer whose properties match the definition of seawater age. As in work by Haidvogel and Bryan [1992] and England [1995b], the model water age (A) can be defined according to the equation

$$dA/dt = L(A) + 1 \quad (3)$$

where $L(A)$ refers to the standard tracer diffusion (and, implicitly, convection) terms in the model and where A obeys the boundary condition

$$A(x, y, z) = 0 \quad (4)$$

at the upper model level and the initial condition $A(x, y, z) = 0$ over the entire model domain. In effect, A is incremented by the model time step during each time step, with the only processes limiting the indefinite growth of A associated with the ventilation of the ocean interior by water originating from the sea surface. By definition, water in direct contact with the sea surface (i.e., the upper model level) retains an age of zero throughout the model integration. Regions of persistent surface convective overturn acquire near-zero age during winter-time months, since the surface age signal is overturned on short timescales (the model time step is just over 1 day) during the convection process.

In an equilibrated state the age tracer (A) measures the volume-weighted timescale at which any point in the ocean interior communicates with the sea surface. In a primitive equation ocean model the source water of any given grid box will be some finite combination of waters that originate from the surface model level. The final equilibrated age of any interior grid box will then be derived from a combination of these finite (though potentially very large) number of sources having a variety of ventilation timescales. For example, water in the deep equatorial Atlantic might have a true age mixture of 200 years, though this could be a complex combination of water as young as 20 years, with additional components of varying age up to perhaps 1000 years old [England, 1995b]. Very old water can exist when a specific water parcel undergoes many recirculations within a given basin or around the circumpolar ocean, without being upwelled or convected into the surface mixed layer. Such water might age significantly before enter-

ing a slow pathway into a quiescent part of the world ocean, where it is destined (through the lack of any strong ambient circulation) to reside in the deep ocean for a very long time.

The age tracer is of little value until the entire age field is completely equilibrated. To ensure that A represents the true age of the model water mass mixtures, the age experiments are run until little change in age is detected throughout the model domain (a criterion of < 6 -months aging per 100-years integration is required over all model grid points). The five model experiments take between 3000 years (experiment ISOP) and 6000 years (experiment GM) to meet this criterion, with the oldest water mass mixture consistently being located in the deep Pacific Ocean. In contrast, the Atlantic Ocean equilibrates over somewhat shorter timescales.

4. CFC Uptake and Outflow in the DWBC

Significant levels of dissolved CFC-11 were first detected in the DWBC by Weiss *et al.* [1985] (see Figures 3a and 4a). Their measurements confirm the presence of CFC-enriched waters at the western boundary of the tropical Atlantic Ocean, with equatorial CFC-11 concentrations reaching $0.05 \text{ pmol kg}^{-1}$ near 1600-m depth by early 1983. The corresponding maps of simulated CFC-11 concentration in the DWBC in each of the model experiments are included in Figures 3 and 4. The CFC data are sampled from the model ocean during early 1983 in order to correspond with the equivalent measurements made by Weiss *et al.* [1985]. In Figure 3 the maps are chosen on those geopotential surfaces that coincide with the core of the DWBC in each case, which varies in depth from 1228 m (experiment GM) to 2228 m (experiment NAW) (see also Figure 4). This is more appropriate than choosing the same density level as that selected by Weiss *et al.* [1985], since the model deep water is generally somewhat less dense than observed. In addition, the Weiss *et al.* [1985] $\sigma_{1.5} = 34.63 \text{ kg m}^{-3}$ density surface was selected to cut through the core of the maximum CFC signal in the DWBC. To reveal the depth structure of the CFC-bearing core in each model case, Figure 4 shows the corresponding latitude-depth section of CFC near the equator (the section location is drawn in Figure 3a).

Except for the NAW and TOPO cases the model runs exhibit much weaker CFC-11 concentrations in the western boundary outflow compared with observations. In effect, the model southward extension of the CFC-enriched upper NADW does not match observations in experiments CTRL, ISOP, and GM. An unrealistically weak deep signal of CFC-11 is seen in the latitude-depth section off South America in experiments CTRL and GM (Figures 4b and 4d), and in experiment ISOP the deep signal is not in the DWBC because of excessive mixing in that case (Figure 4c). The DWBC is deficient in CFC-11 in these three model cases because the timescale for NADW outflow is too slow. The long timescale is primarily due to unrealistically sluggish deep currents, particularly in the case with Gent *et al.* [1995] tracer diffusion (experiment GM; Figure 3d). In addition, in all model runs, part of the path of NADW outflow includes a questionable loop eastward from the Labrador Sea into the northeastern Atlantic Basin, effectively increasing the required outflow journey by around 4000 km [England *et al.*, 1994]. The additional circulation eastward ages the water mass by at least 8 years (depending on the speed of the model ocean currents), thereby yielding significantly lower CFC concentrations in the NADW extension.

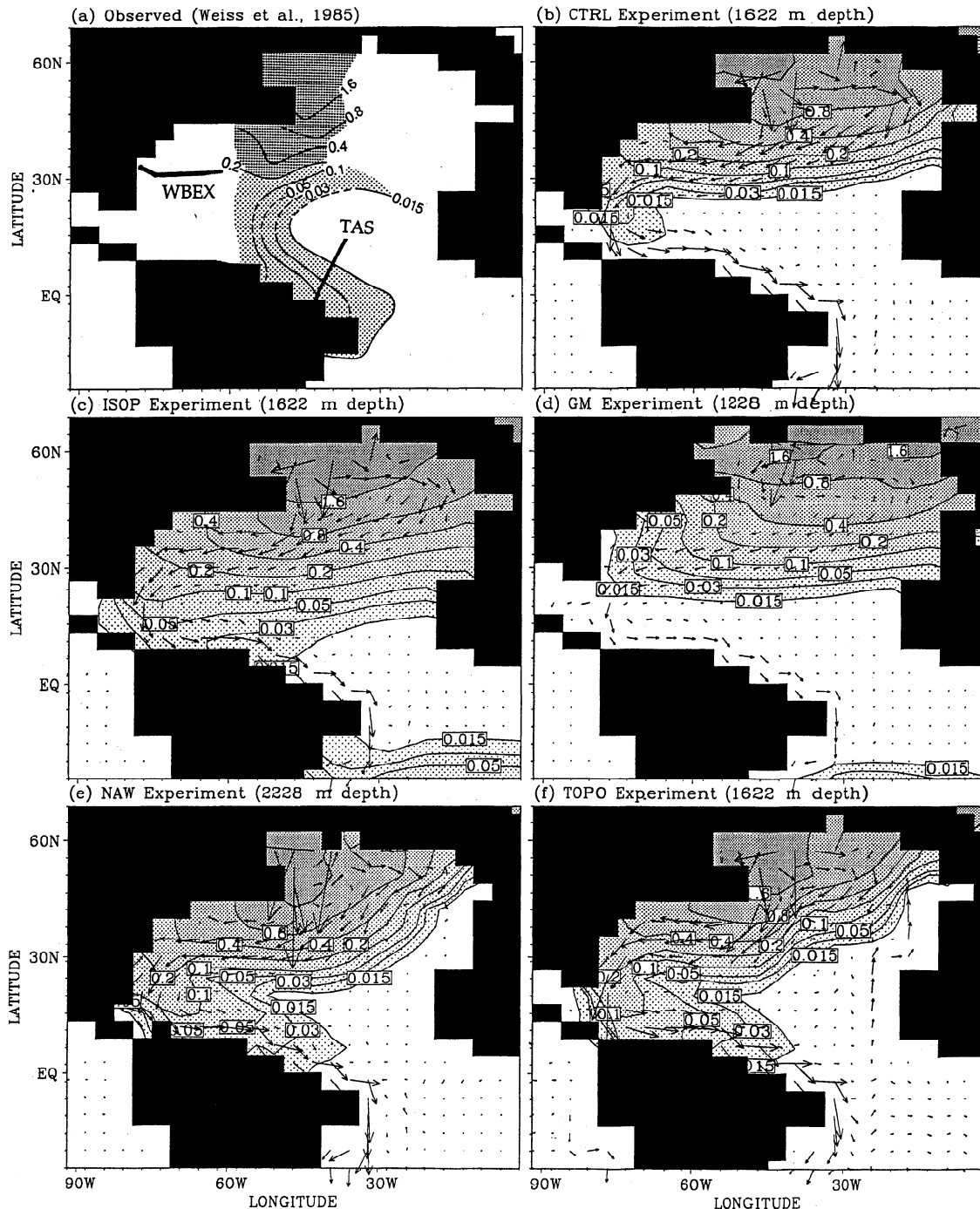


Figure 3. (a) Observed CFC-11 on the $\sigma_{1.5} = 34.63 \text{ kg m}^{-3}$ density surface measured during December 1982 to February 1983 as part of the Transient Tracers in the Ocean (TTO) program (redrafted from Weiss *et al.* [1985]). The density surface was selected by Weiss *et al.* [1985] to cut through the maximum southward extension of the CFC signal in the Deep Western Boundary Current (DWBC). (b-f) Simulated model currents and CFC-11 at the depth of maximum CFC content in the DWBC during February 1983. Contour levels are drawn at standard concentrations. In Figure 3a we indicate the location of the Tropical Atlantic Study (TAS) and Western Boundary Exchange Experiment (WBEX) sections plotted in Figures 4 and 7.

The outflowing CFC-11 signal is far too diffuse in the isopycnal mixing experiment (Figure 3c), having little zonal structure, even though the outflow currents are predominantly at the western boundary. Model data sampled during later years confirm that all other experiments simulate an outflowing signal along the western boundary of the deep

tropical Atlantic, whereas the isopycnal mixing case diffuses much of this signal eastward. The inclusion of an isopycnal mixing scheme without a substantial reduction in background horizontal mixing can therefore introduce significant errors in the simulated ventilation of the ocean model in the North Atlantic.

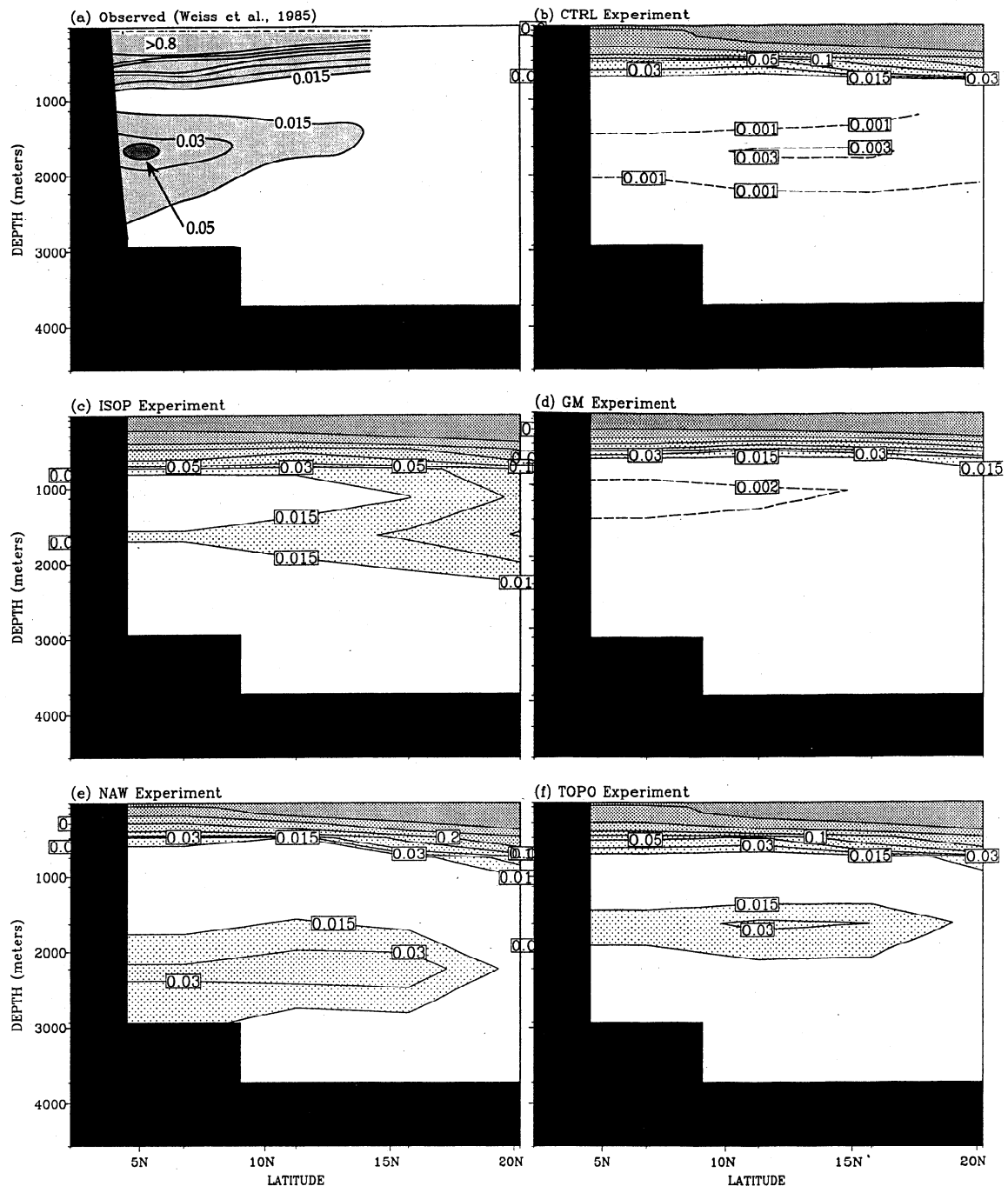


Figure 4. (a) Observed CFC-11 on the Tropical Atlantic Study (TAS) section extending from near the South American continent at the equator northeastward toward the Mid-Atlantic Ridge, as shown in Figure 3a (redrafted from Weiss *et al.* [1985]). (b-f) Corresponding sections of simulated CFC-11 in each model case during February 1983. Contour levels are drawn at the standard values, with an additional set of weaker CFC-11 concentrations shown in the DWBC in experiments control (CTRL) and Gent and McWilliams [1990] (GM).

The GM experiment shows a great reduction in model ocean current speeds in the DWBC, with the current decreasing in strength from typically 2.0 cm s^{-1} (CTRL) to $1.0\text{--}1.5 \text{ cm s}^{-1}$ (GM). The net meridional overturning in the North Atlantic is generally shallower and weaker in the GM case (Figure 5), although there is a reduction in the spurious western boundary upwelling as noted by Böning *et al.* [1995]. Under GM, NADW outflow is confined to only the upper 1600 m, in contrast to the deep outflow noted in observations [e.g., Smethie,

1993]. In addition, flattened isopycnal surfaces in the GM run reduce the strength of interior geostrophic flows. This acts to reduce the speed of flow in the DWBC in an already viscous model with sluggish deep currents. A spatially varying coefficient for the GM isopycnal thickness diffusion term such as that advocated by Visbeck *et al.* [1997], one that depends on vertical and horizontal stratification, might yield substantially different baroclinic currents in the region.

The enhanced wintertime *T-S* restoration in experiment

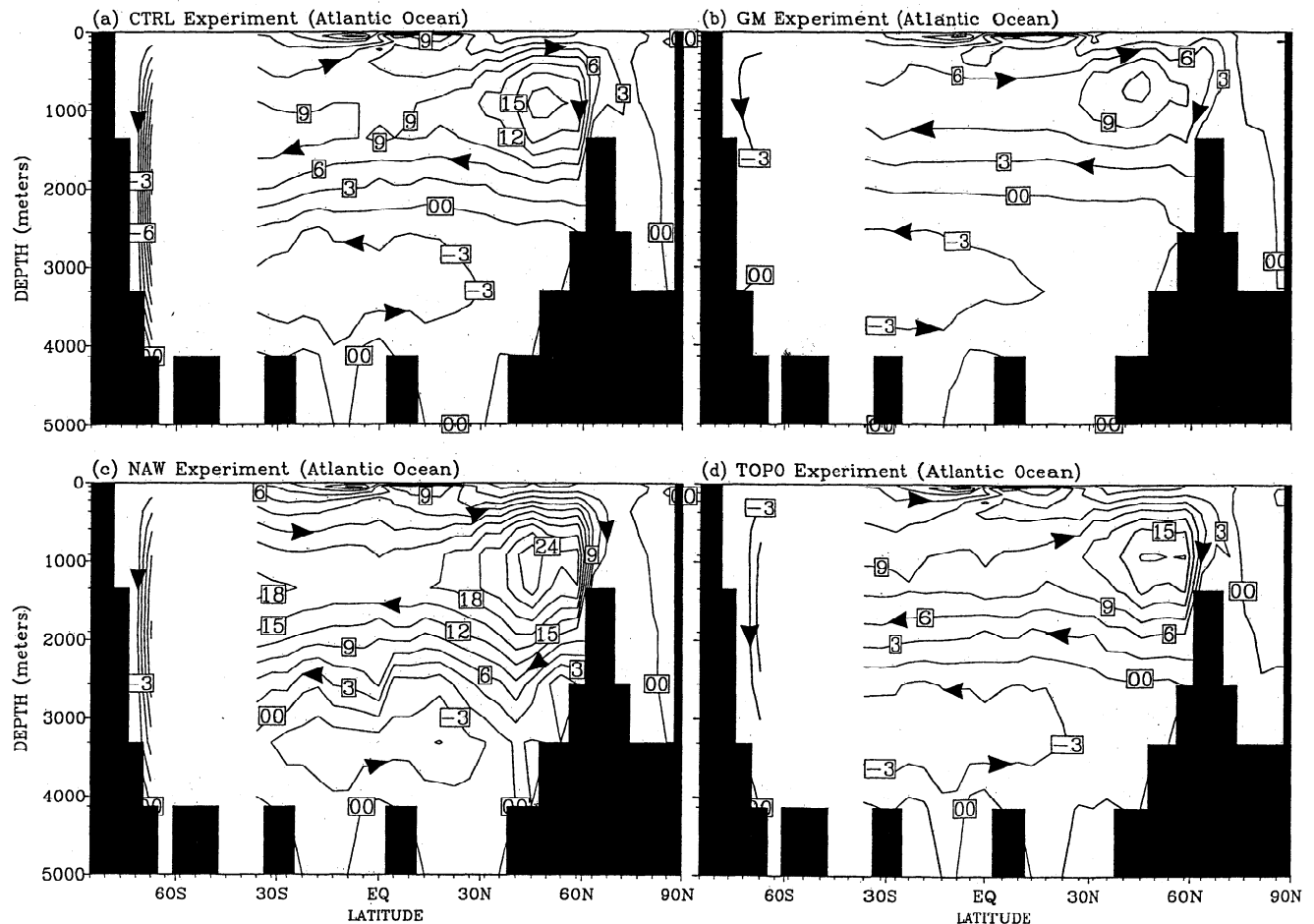


Figure 5. Annual mean meridional overturning (in Sverdrups (Sv), $1 \text{ Sv} = 10^6 \text{ m}^3 \text{ s}^{-1}$) in the Atlantic Ocean in experiments (a) CTRL, (b) GM, (c) North Atlantic winter (NAW), and (d) topographic stress (TOPO). No contours are drawn where the model is zonally unbounded. Contours are drawn at intervals of 3 Sv. Meridional overturning values shown for GM include the additional tracer advection transports of *Gent et al.* [1995].

NAW increases the production rate of NADW to 28.5 Sv (from 20.1 Sv in the CTRL), and the outflow transport also increases (from 8.5 Sv in CTRL to 17.3 Sv in NAW, see Figure 5). Here we define NADW “production rate” as the maximum value of the meridional overturning in the North Atlantic, and the “outflow rate” as that part of NADW that flows into the Southern Ocean. Errors resulting from this definition due to zonal recirculations are negligible in all model cases except experiment TOPO (see also Figure 6). Corresponding to the more vigorous overturn in experiment NAW, the CFC-11 burden in outflowing NADW is enhanced, with a clear signal in the Western Boundary Current off South America by 1983 (Figures 3e and 4e). The core of the outflowing CFC signal has deepened from 1622 m (CTRL) to 2228 m (NAW), with more direct flow of CFC-enriched Labrador Sea Water flowing southward from the convection zone (instead of looping eastward into the northeastern Atlantic Basin). This has the net effect of enhancing the CFC-11 content in the DWBC in broad agreement with the observed sections of *Weiss et al.* [1985]. However, as noted earlier, our technique of enhancing the T - S restoring terms implies unrealistically large heat and freshwater fluxes in the North Atlantic during winter. In effect, the model circulation is being corrected using artificial surface-forcing fields.

In experiment TOPO the speed of the DWBC intensifies, and less LSW flows eastward toward the northeastern Atlantic Basin. Even the water that does loop eastward recirculates southward after a shorter excursion (compare the model currents in cases TOPO and CTRL, Figure 3). In addition, a poleward flowing Deep Eastern Boundary Current is simulated in TOPO, which is free of anthropogenic CFC-11, thereby weakening the net CFC content in the northeastern Atlantic Basin. The *Weiss et al.* [1985] sections do not extend eastward of 40°W at these latitudes, so we cannot determine whether this is an improvement in the model simulation. Nevertheless, it is clear that the TOPO parameterization improves the CFC modeled in the DWBC, with a narrower and more enriched CFC-11 signal off South America by early 1983.

It is worth noting that in TOPO the apparent outflow of NADW in the map of meridional overturning (Figure 5) is somewhat weaker than the actual DWBC transport. Figure 6 shows a longitude-depth section of north-south velocities at 25°N in both the CTRL and TOPO cases. Northward velocities in excess of $10^{-3} \text{ cm s}^{-1}$ are stippled. Away from the DWBC in case CTRL, only very weak ocean currents are noted (see also Figure 3). In contrast, a significant northward flowing Eastern Boundary Current is simulated in TOPO. On taking a zonal mean of ocean transport as is done when constructing

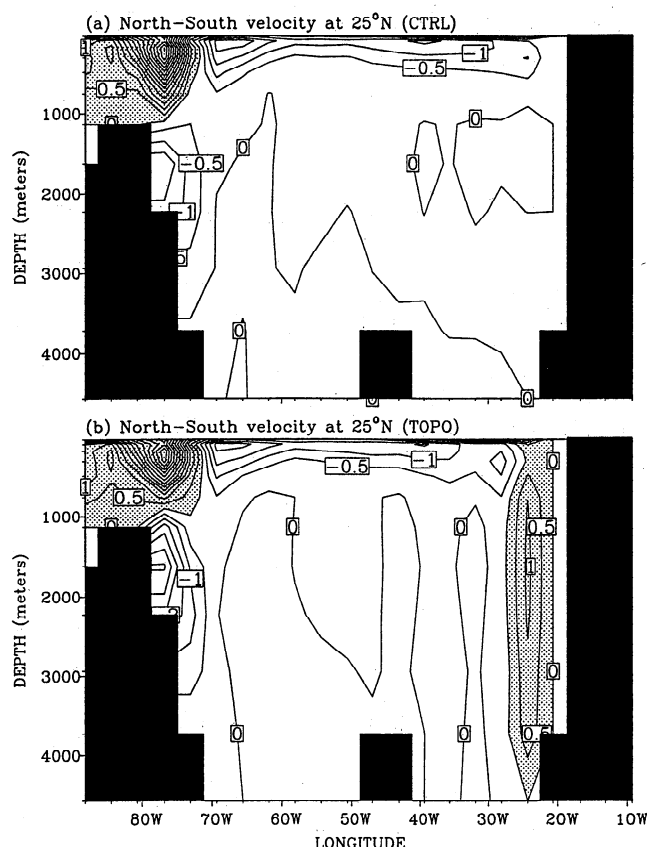


Figure 6. Longitude-depth section of meridional velocity (cm s^{-1}) at 25°N for experiments (a) CTRL and (b) TOPO. Stippled regions denote northward currents in excess of $10^{-3} \text{ cm s}^{-1}$.

the meridional overturn, part of the DWBC is aliased by this northward flow. In effect, the actual DWBC transport in TOPO (13.7 Sv) appears in the meridional overturning map as a weaker outflow of NADW (9.2 Sv). Care should therefore be taken when extrapolating NADW outflow rates from a consideration of the meridional transport stream function alone.

Farther upstream in the outflowing NADW ($32^\circ\text{--}45^\circ\text{N}$), *Smethie* [1993] finds two distinct layers of CFC near the continental slope (Figure 7a), one in Upper NADW near 800- to 1500-m depth and one in Lower NADW at about 3500-m depth, the upper maximum feeding the CFC core detected in the *Weiss et al.* [1985] $\sigma_{1.5} = 34.63 \text{ kg m}^{-3}$ density surface of Figure 3a. The deeper core originates from dense water with classical NADW properties overflowing the Greenland-Iceland-Scotland Ridge [*Smethie*, 1993], a feature not typically resolved by coarse-resolution ocean models [e.g., *Toggweiler et al.*, 1989; *England*, 1993; *Hirst and Cai*, 1994]. Figure 7 includes the model simulations of CFC-11 at WBEX stations 22-38 during April-May 1986, corresponding to the observed section of *Smethie* [1993]. Clearly apparent in the model-observation comparison is the absence of any deeper CFC-burdened NADW. The absence of any CFC in Lower NADW is related to the shallow meridional overturning cells simulated in the model (Figure 5), with little contribution of dense water overflowing the Greenland-Iceland-Scotland Ridge. Some experiments were rerun with a much deepened ridge topography; little change in meridional overturning was noted. It is likely that substantially higher horizontal and vertical resolutions are required for the model to capture this

dense water overflow signature [see, e.g., *Böning et al.*, 1996]. In contrast, all model cases capture a shallower core of CFC underlying the layer of minimum CFC, with the exception perhaps of GM. This shallower core in the model tends to be broader and more diffuse than observed.

Other experiments were undertaken to examine CFC outflow in the DWBC in different model cases or in certain

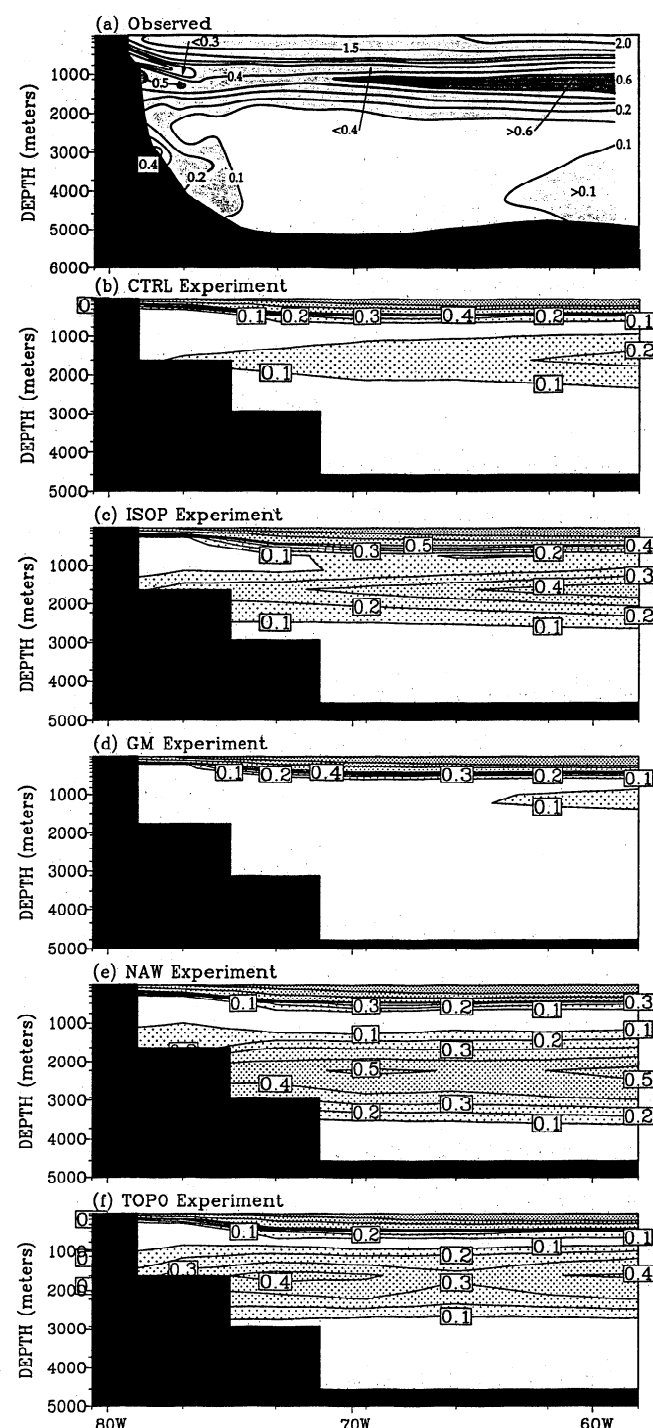


Figure 7. (a) Vertical section of observed CFC-11 along WBEX stations 22-38 near $32^\circ\text{--}34^\circ\text{N}$ (redrafted from *Smethie* [1993]). The WBEX section location is indicated in Figure 3a. CFC-11 concentrations $> 0.5 \text{ pmol kg}^{-1}$ are densely stippled. (b-f) Corresponding sections of simulated CFC-11 in each model case during April-May 1986. Contour levels are drawn at 0.1, 0.2, 0.3, 0.4, 0.5, 0.6, 1.0, 1.5, and 2.0 pmol kg^{-1} .

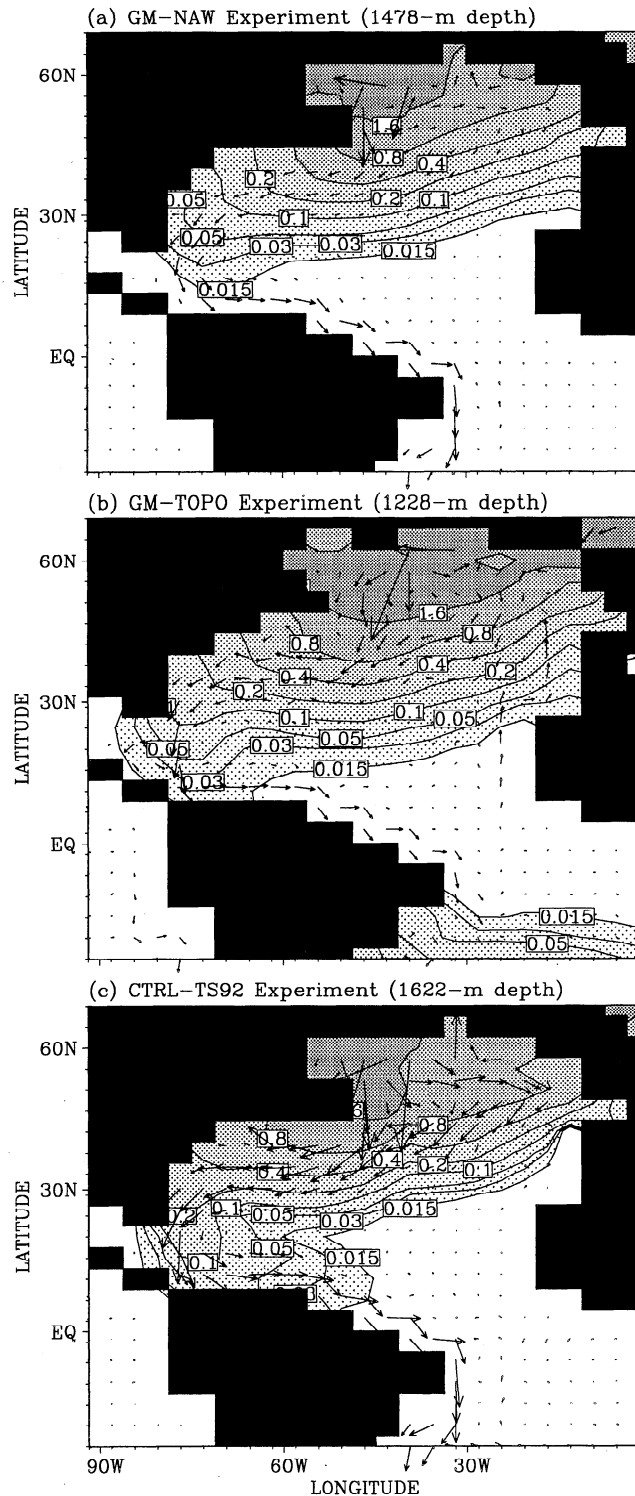


Figure 8. Simulated model currents and CFC-11 at the depth of maximum CFC content in the DWBC during February 1983 in three ancillary experiments: (a) the GM case with NAW surface thermohaline forcing, (b) the GM case including a topographic stress parameterization (TOPO), and (c) the CTRL case with Southern Ocean wind stress increased by 50% (as examined by Toggweiler and Samuels [1992]).

combinations of the main experiments considered above (Figure 8). In the first instance the GM and NAW cases were combined. Even when GM is rerun with an enhanced wintertime T - S restoration, the outflowing CFC-11 signal is

still somewhat weaker than Weiss *et al.* [1985] observe. The same is true in a model simulation that combined the GM and TOPO cases (Figure 8b). Even though some improvement in the CFC simulation is achieved in the new GM runs, the outflow transport is still too weak and shallow. In a final experiment the Southern Ocean wind stress in CTRL was increased by 50% as in Toggweiler and Samuels [1992], resulting in a more vigorous production rate and overturn of

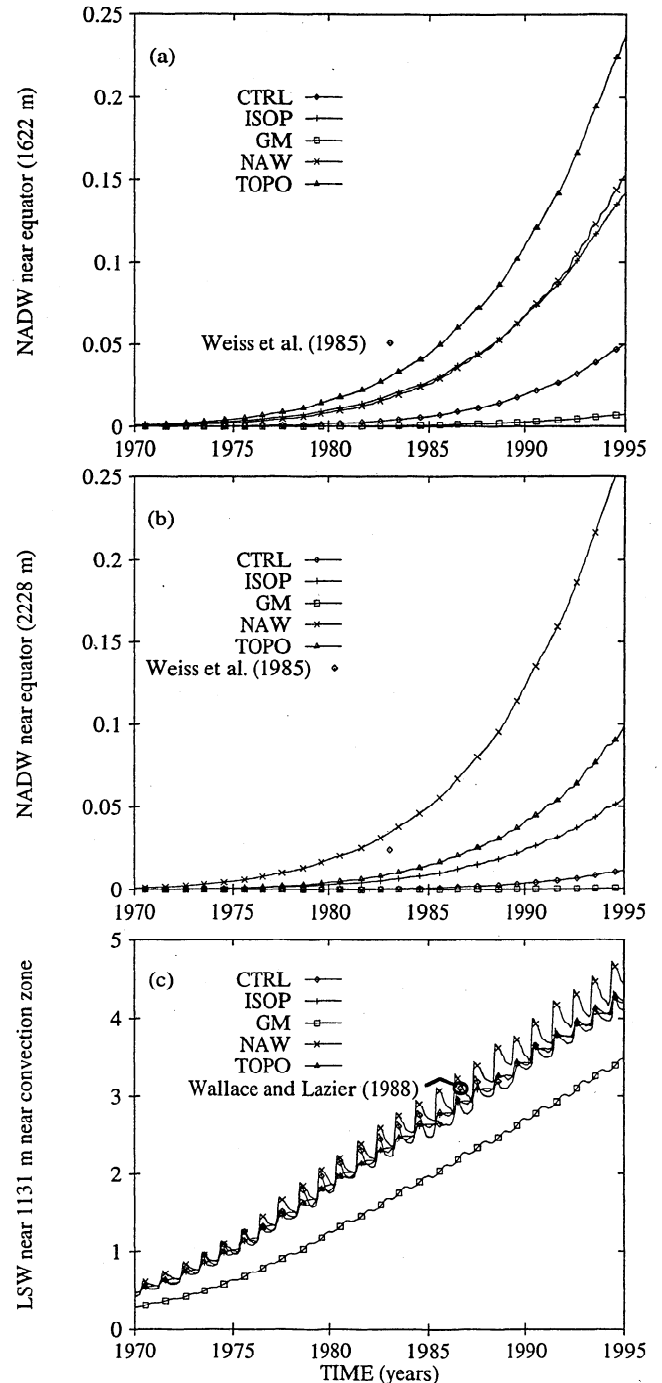


Figure 9. Time series of simulated CFC-11 concentration (pmol kg⁻¹) of water in the DWBC at the equator at (a) 1622-m depth, (b) 2228-m depth, and (c) in the Labrador Sea convection region near 1000-m depth. Values for the GM case are taken as the maximum values at the corresponding two model grid levels. Where available, observational data are included for direct comparison.

Table 3. Simulated and Observed CFC-11 Content and Seawater Age in the Deep Western Boundary Current at the Equator During February 1983

Experiment:	Depth, m	CFC-11, pmol kg ⁻¹	CFC Age, years	Equilibrated Age, years
CTRL	1622	0.006	32	167
ISOP	1622	0.027	25	141
GM	1228	0.003	33	210
NAW	2228	0.049	27	148
TOPO	1622	0.044	27	190
Observed	1600	0.051	23	...

The CFC observations are taken from *Weiss et al.* [1985]. The estimates of equatorial DWBC age are derived from either the CFC-11/CFC-12 ratio or from the idealized age tracer A. The depth levels chosen in each experiment are those with maximum equatorial signatures of CFC-11 in the DWBC (as in Figures 3, 10, and 11).

NADW. The outflowing CFC signal in this run is nearly as strong as the NAW and TOPO cases, although like NAW, this is achieved by unrealistic surface forcing conditions.

The transient penetration of CFC-tagged waters in the DWBC can be plotted as a function of time. In Figure 9 we show the maximum signal of CFC-11 in the core of the DWBC at the equator for each experiment at model levels 8 and 9 (1622 m and 2228 m, respectively). The GM values are taken as the maximum values in the corresponding two model levels near these depths (recalling that in GM, all deeper model levels are split into two levels for numerical stability). The observed signal measured by *Weiss et al.* [1985] is also indicated in these diagrams, and model to observation comparisons are presented in Table 3. For reference, a similar figure is shown for the CFC-11 content in the LSW convection region near 1000-m depth (Figure 9c). The CFC uptake in the Labrador Sea convection region is similar in all model cases except for GM, where substantially less convection occurs in the region [England and Hirst, 1997]. A clear seasonal cycle in uptake in the winter mixed layer is apparent in all model cases. Strongest CFC-11 signals in newly formed LSW are noted in experiment NAW, since in that case, deep water overturn is greatest.

Even though CFC-11 content in the deep Labrador Sea is rather similar in four of the five model cases (and in good agreement with the observations of *Wallace and Lazier* [1988]), quite different concentration time series are noted near the equator. This is because different DWBC pathways and transports are simulated in each of the model experiments. Overall, the TOPO and NAW cases exhibit the most realistic CFC-11 burdens in the DWBC. At 1622-m depth, all model cases underestimate the CFC content in the DWBC (experiment TOPO being the closest to realistic), whereas at 2228-m depth, experiment NAW overestimates the outflowing signal (all other cases underestimate the outflow of CFC at this depth). The CTRL and GM cases are the most spuriously deficient in CFC-11 in the DWBC at the equator. The ISOP case appears to have more realistic CFC-11 samples in the deep outflowing current, though this is primarily due to artificially rapid blending of water mass properties by the isopycnal diffusion terms, not the correct simulation of the DWBC (see, e.g., Figures 3c and 4c). The TOPO and NAW experiments carry the most realistic amount of CFC-11 in the Deep Boundary Current (Table 3), owing to more realistic current speeds and outflow pathways of LSW in these model cases.

5. Seawater Age in the DWBC

Maps of the estimated seawater age derived from the ratio of CFC-11 to CFC-12 are drawn for each of the model cases in Figure 10. The depth levels chosen correspond to the maximum outflow signal of CFC-11 in each model case (as in Figure 3). For direct comparison the equilibrated age tracer A is shown at the corresponding model depths in Figure 11. Included in each case is some indication of observed estimates of seawater age using different seawater dating techniques. In Figure 10a we show estimates of seawater age in the DWBC made from observations of the CFC-11/CFC-12 ratio [*Weiss et al.*, 1985; *Doney and Bullister*, 1992; *Smethie*, 1993]. In Figure 11a we show the radiocarbon estimate of age at 3000-m depth made by *Broecker et al.* [1988]. Even though the radiocarbon age estimates were derived at a depth somewhat deeper than our selected model levels, similar circulation patterns at 3000-m depth in the real ocean suggest that the *Broecker et al.* [1988] estimates are at least qualitatively applicable for a depth range of 1500 to 4500 m (i.e., those depths that witness the outflow of NADW in the western boundary). A summary of the age estimates of water in the DWBC at the equator is included in Table 3.

The most striking feature of the age analyses shown in Figures 10 and 11 is that the CFC ratio estimates of age are substantially younger than the equilibrated age tracer in all cases. This is simply because the CFC ratio estimates are essentially appropriate for the younger variety of source waters feeding the DWBC (i.e., those having detectable traces of CFC-11 and CFC-12), whereas the equilibrated age tracer includes all source waters, from the very young CFC-burdened waters through to any traces of recirculated waters that have zero CFC content. The CFC-free waters cannot weaken the CFC-11/CFC-12 ratio (and thereby increase the age estimate), whereas they will contribute to greater values of the idealized age tracer A. Caution is therefore warranted when extrapolating age estimates of water mass mixtures from the CFC ratio alone, particularly when some degree of dilution with CFC-free waters has occurred.

Youngest waters at the level of the DWBC are confined to the northern North Atlantic (particularly near the Labrador Sea), with water masses aging gradually in the outflow currents. The broad structure of age is similar in both the CFC ratio and idealized age estimates (where the CFC estimates are defined). For example, weaker zonal structure in age is seen in the northern North Atlantic in experiments CTRL, ISOP, and

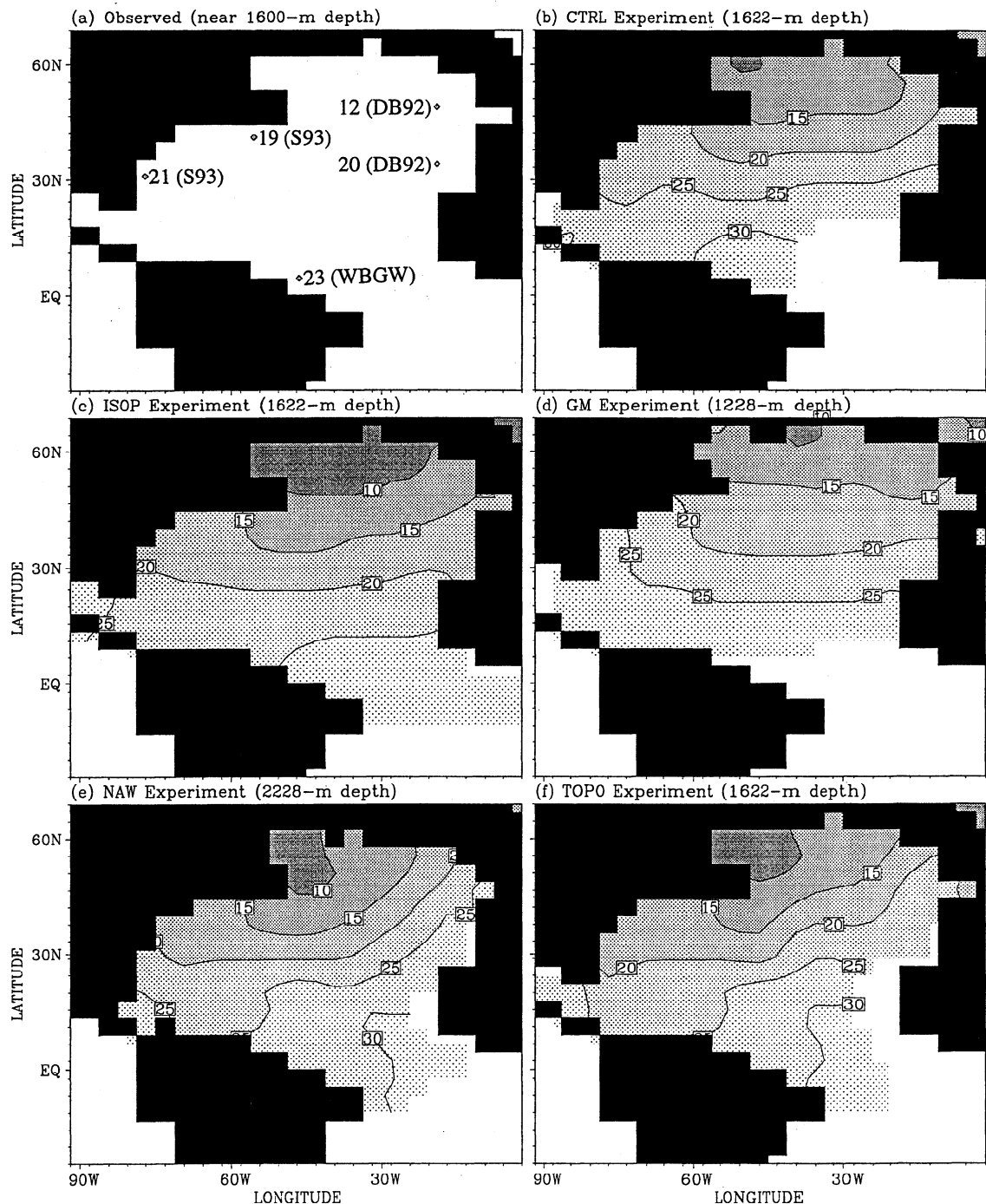


Figure 10. Estimated seawater age (years) derived from the CFC-11/CFC-12 ratio. (a) Observed estimates from Weiss *et al.* [1985] (WBGW), Doney and Bullister [1992] (DB92), and Smethie [1993] (S93). (b-f) Estimates derived from the five model experiments at the levels of maximum CFC burden in the DWBC. No age values are given where CFC-11 or CFC-12 content is weaker than $0.005 \text{ pmol kg}^{-1}$.

GM compared with cases NAW and TOPO. Only a weak signal of the DWBC is apparent in experiment ISOP in both estimates of age, even though the outflow current is on the western boundary (see Figure 3c). Oldest North Atlantic waters in all model cases appear near the tropics in the eastern boundary, although a poleward flowing eastern boundary current in experiment TOPO spreads this old water northward. This feature of the TOPO case is quite distinct from the other model experiments.

There is some qualitative disagreement between the CFC ratio age and the equilibrated age tracer in the five experiments. For example, the equatorial DWBC waters in experiment TOPO are relatively young according to the CFC ratio (27 years) and, in contrast, quite old in the equilibrated age tracer (190 years). This is because that case exhibits realistically swift currents in the DWBC outflow (leading to a reasonable agreement in CFC age with Weiss *et al.* [1985]), although its dilution rate with older waters must be higher to attain an old equilibrated

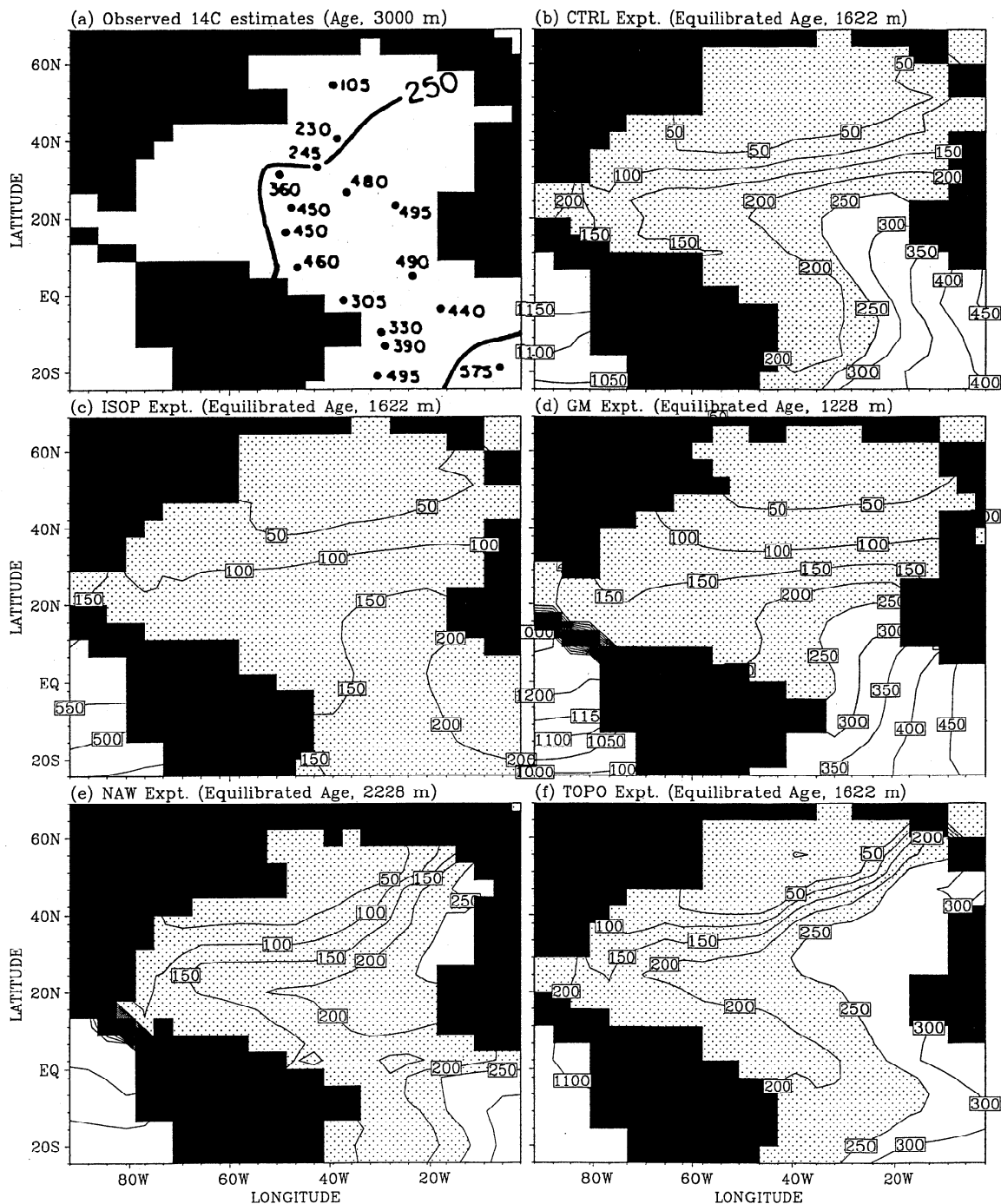


Figure 11. (a) Radiocarbon-derived estimates of water age (years) at 3000-m depth in the Atlantic Ocean, as estimated by Broecker *et al.* [1988] referencing $^{14}\text{C}/^{12}\text{C}$ ratios at 3-km depth relative to those of the overlying surface water. (b-f) Equilibrated idealized age tracer (years) in the five model cases at the depth of maximum CFC burden in the DWBC.

age. This is likely to originate from the older CFC-free waters flowing poleward at the eastern boundary in that model case (Figure 3f). These waters cannot dilute the CFC ratio, although they will contribute to an older equilibrated age in the DWBC.

6. Conclusions

A number of configurations of the GFDL ocean general circulation model have been integrated with CFC uptake in order

to study the simulation of the DWBC in the North Atlantic. The five principal versions cover three different parameterizations of subgrid-scale mixing (standard Cartesian, isopycnal, and the eddy advection scheme of Gent *et al.* [1995]), a version with enhanced surface thermohaline forcing, and, finally, a case that incorporates the effects of topographic stress as in the study of Alvarez *et al.* [1994]. It was shown that only two of the five model cases simulate realistic burdens of CFC-11 in Upper NADW, namely, the case with enhanced surface T - S forcing (NAW) and the case

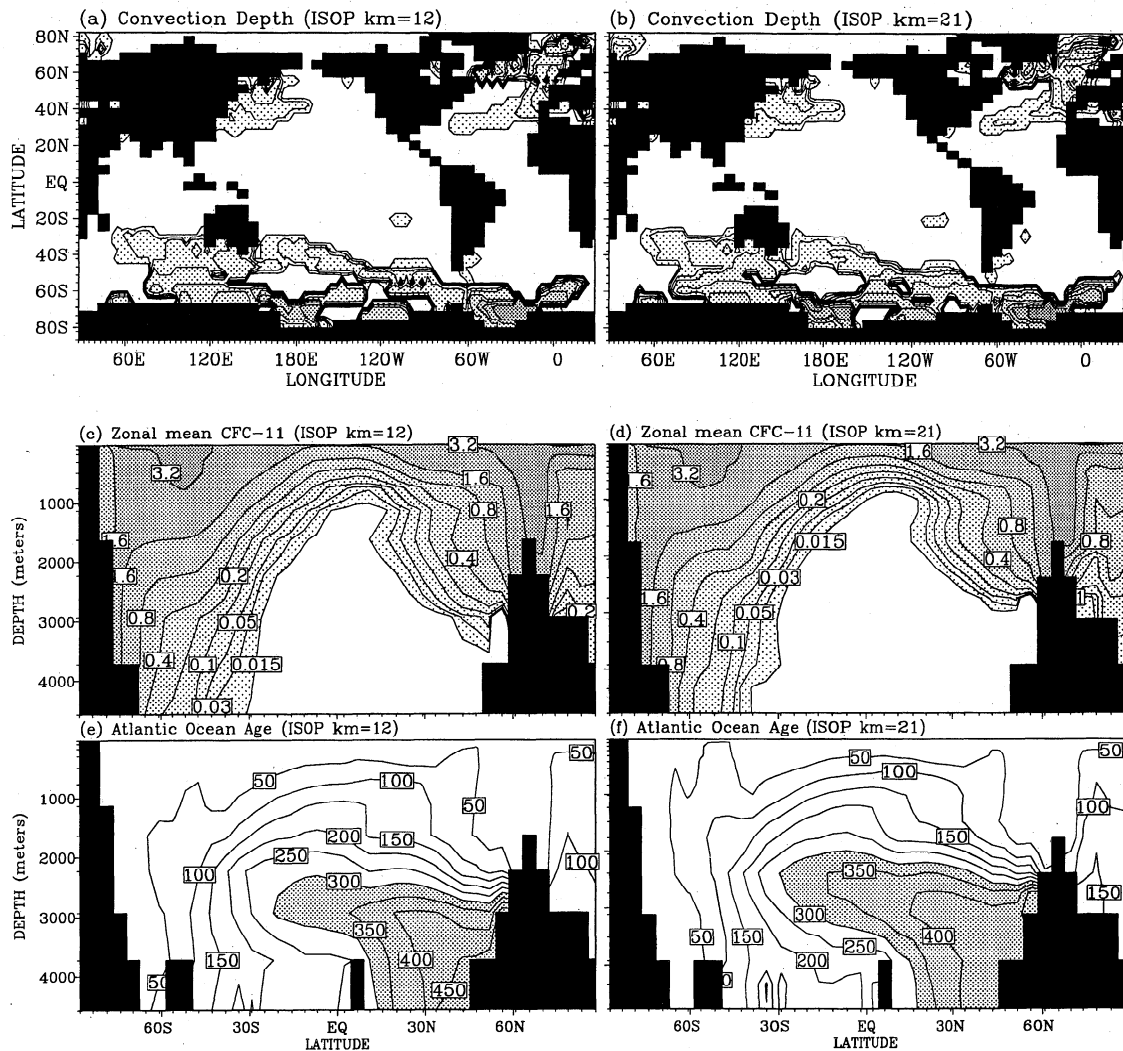


Figure A1. Comparison of key ventilation diagnostics in the ISOP experiment run with 12 and 21 vertical levels. (a, b) Wintertime surface level convective overturn (in meters); contours are drawn at depths of 120, 240, 400, 600, 1000, 1400, 1900, 2600, 3400, and 4200 m. (c, d) Global zonal mean CFC-11 (pmol kg^{-1}) simulated during 1991, and (e, f) equilibrated seawater age (years) in the Atlantic sector.

incorporating the effects of topographic stress (TOPO). These two cases exhibit more direct southward outflow of LSW from the convection region and faster current speeds in the western boundary flow. However, the model run with a tightly constrained T - S forcing was diagnosed to have unrealistic surface heat loss and large freshwater fluxes during winter as a result of the short restoring timescales imposed. Therefore it cannot be recommended as a technique for increasing NADW production in ocean circulation models, particularly when these models are used for coupled climate studies.

The CFC-11 burden simulated in the LSW convection zone is quite realistic in two of the three model cases that exhibit deficient CFC in Upper NADW (experiments CTRL and ISOP). This implies that these two model cases capture LSW convection well, and yet they poorly reproduce the speed and outflow path of the DWBC. Experiment ISOP also displays a very broad and diffuse CFC-11 signal in the North Atlantic, even though the outflow currents are predominantly at the western boundary. This is because of excessive tracer mixing in that run. In contrast, the *Gent et al.* [1995] case (GM) exhibits

only weak tracer diffusion, but its simulated outflow currents are very weak and generate only a sluggish outflow of CFC-tagged LSW. Our adopted value of $\kappa = 1.0 \times 10^7 \text{ cm}^2 \text{ s}^{-1}$ for the thickness diffusion coefficient may be inappropriate for the North Atlantic (as suggested by Visbeck et al. [1997]). Additional experiments with a spatially varying GM isopycnal thickness diffusion coefficient are recommended.

None of the model cases capture a deeper layer of CFC near the continental slope corresponding to Lower NADW. In observations the deeper core originates from dense water with classical NADW properties overflowing the Greenland-Iceland-Scotland Ridge [Smethie, 1993]. The absence of any CFC in Lower NADW is related to the shallow meridional overturning cells simulated in the model experiments, with very little contribution of dense water overflowing the Greenland-Iceland-Scotland Ridge. It is likely that substantially higher horizontal and vertical resolutions are required to capture this dense water overflow signature in ocean models [see, e.g., Böning et al., 1996].

Seawater age in the DWBC was estimated in the model

using both the CFC-11/CFC-12 ratio as well as an idealized numerical tracer of age. The CFC ratio estimates are substantially younger than the equilibrated age tracer in all cases. This is because the CFC-derived values are essentially appropriate for the younger variety of source waters feeding the DWBC (i.e., those having detectable traces of CFC-11 and CFC-12), whereas the equilibrated age tracer includes all source waters, from the very young CFC-burdened waters through to older recirculated water having zero CFC content. This leads to some inconsistency in the age estimates, with one model case (experiment TOPO) appearing to have relatively young waters in the DWBC from the CFC ratio and yet appearing to be relatively old when the equilibrated age tracer is considered. Caution is therefore recommended when extrapolating overall seawater age from the ratio of CFC-11 to CFC-12 when significant dilution with CFC-free waters has occurred.

Transient tracers are particularly useful when addressing the problem of simulating the deep outflow in the North Atlantic Ocean. Measurements of CFCs, for example, can be used to determine whether a model is correctly simulating NADW formation rates, outflow pathways, and current speeds. The feasibility of studies such as the present one is critically dependent on past and continued observation of such tracers in the North Atlantic Ocean.

Appendix: Importance of Choice of Vertical Resolution

To explore the importance of adopting low vertical resolution in the non-GM cases, we reran experiments ISOP and CTRL with the same 21 vertical levels adopted in GM. The resulting ventilation rates turn out to be very similar to those found in the low-resolution runs. To demonstrate this, Figure A1 shows the depth of maximum wintertime convection, the simulated zonal mean CFC content during 1991, and the equilibrated model age in case ISOP at both 12- and 21-level resolution. The CFC panel reveals decadal timescale ventilation, whereas the age section shows renewal processes at and beyond centennial timescales. Convection regions and depths are almost identical in the two cases, as is the meridional overturn (not shown). Further, simulated CFC content and model age are very similar, demonstrating that over decadal to centennial timescales the ISOP case is relatively insensitive to the choice of vertical resolution. This is also true of CTRL, and though as yet untested, we expect this to hold for the other non-GM runs.

Acknowledgments. This research was supported by the Australian Research Council and the University of New South Wales Vice-Chancellor's Research Fellowship Scheme. The model computations were carried out on the CSIRO Cray YMP 4E/369 and the University of New South Wales Cray YMP-EL. Ken Caldeira, Robbie Toggweiler, and an anonymous reviewer provided useful comments on an earlier version of the manuscript. MHE gratefully acknowledges funding support from the National Science Foundation, the National Oceanic and Atmospheric Administration, Lamont-Doherty Earth Observatory of Columbia University, and Biosphere 2 for attendance of the Maurice Ewing Symposium.

References

- Alvarez, A., J. Tintore, G. Holloway, M. Eby, and J.M. Beckers, Effect of topographic stress on the circulation in the western Mediterranean, *J. Geophys. Res.*, 99, 16053-16064, 1994.
- Böning, C.W., W.R. Holland, F.O. Bryan, G. Danabasoglu, and J.C. McWilliams, An overlooked problem in model simulations of the thermohaline circulation and heat transport in the Atlantic Ocean, *J. Clim.*, 8, 515-523, 1995.
- Böning, C.W., F.O. Bryan, W.R. Holland, and R. Döschner, Deep water formation and meridional overturning in a high-resolution model of the North Atlantic, *J. Phys. Oceanogr.*, 26, 1142-1164, 1996.
- Broecker, W.S., The great ocean conveyor, *Oceanography*, 4, 79-89, 1991.
- Broecker, W.S., M. Andree, G. Böhani, W. Woelfli, H. Oeschger, M. Klas, A. Mix, and W. Curry, Preliminary estimates for the radiocarbon age of deep water in the glacial ocean, *Paleoceanography*, 3, 659-699, 1988.
- Bryan, F.O., Parameter sensitivity of primitive equation ocean general circulation models, *J. Phys. Oceanogr.*, 17, 970-985, 1987.
- Bryan, K., A numerical method for the study of the circulation of the world ocean, *J. Comput. Phys.*, 3, 347-376, 1969.
- Bryan, K., and L.J. Lewis, A water mass model of the World Ocean, *J. Geophys. Res.*, 84, 2503-2517, 1979.
- Comiso, J.C., C.R. McClain, C.W. Sullivan, J.P. Ryan, and C.L. Leonard, Coastal zone color scanner pigment concentrations in the Southern Ocean and relationships to geophysical surface features, *J. Geophys. Res.*, 98, 2419-2451, 1993.
- Cox, M.D., A primitive equation, three-dimensional model of the ocean, *GFDL Ocean Group Tech. Rep.* 1, 143 pp., Geophys. Fluid Dyn. Lab. Ocean Group, Princeton, N.J., 1984.
- Danabasoglu, G., and J.C. McWilliams, Sensitivity of the global ocean circulation to parameterizations of mesoscale tracer transports, *J. Clim.*, 8, 2967-2987, 1995.
- Danabasoglu, G., J.C. McWilliams, and P.R. Gent, The role of mesoscale tracer transports in the global ocean circulation, *Science*, 264, 1123-1126, 1994.
- Doney, S.C., and J.L. Bullister, A chlorofluorocarbon section in the eastern North Atlantic, *Deep Sea Res., Part A*, 39, 1857-1883, 1992.
- Döschner, R., C.W. Böning, and P. Herrmann, Response of meridional overturning and heat transport in the North Atlantic to changes in thermohaline forcing at northern latitudes: A model study, *J. Phys. Oceanogr.*, 24, 2306-2320, 1994.
- Eby, M., and G. Holloway, Sensitivity of a large-scale ocean model to a parameterization of topographic stress, *J. Phys. Oceanogr.*, 24, 2577-2588, 1994.
- England, M.H., Representing the global-scale water masses in ocean general circulation models, *J. Phys. Oceanogr.*, 23, 1523-1552, 1993.
- England, M.H., Using chlorofluorocarbons to assess ocean climate models, *Geophys. Res. Lett.*, 22, 3051-3054, 1995a.
- England, M.H., The age of water and ventilation time-scales in a global ocean model, *J. Phys. Oceanogr.*, 25, 2756-2777, 1995b.
- England, M.H., and A.C. Hirst, Chlorofluorocarbon uptake in a world ocean model, 2, Sensitivity to surface thermohaline forcing and subsurface mixing parameterizations, *J. Geophys. Res.*, 102, 15709-15731, 1997.
- England, M.H., V.C. Garçon, and J.-F. Minster, Chlorofluorocarbon uptake in a world ocean model, 1, Sensitivity to the surface gas forcing, *J. Geophys. Res.*, 99, 25215-25233, 1994.
- Esbenson, S.K., and Y. Kushnir, The heat budget of the global ocean: An atlas based on estimates from surface marine observations, *Rep.* 29, Clim. Res. Inst., Oregon State Univ., Corvallis, Oregon, 1981.
- Gammon, R.H., J. Cline, and D. Wisegarver, Chlorofluoromethanes in the northeast Pacific Ocean: Measured vertical distributions and application as transient tracers of upper ocean mixing, *J. Geophys. Res.*, 87, 9441-9454, 1982.
- Gent, P.R., and J.C. McWilliams, Isopycnal mixing in ocean circulation models, *J. Phys. Oceanogr.*, 20, 150-155, 1990.
- Gent, P.R., J. Willebrand, T.J. McDougall, and J.C. McWilliams, Parameterizing eddy-induced tracer transports in ocean circulation models, *J. Phys. Oceanogr.*, 25, 463-474, 1995.
- Haidvogel, D.B., and F.O. Bryan, Ocean general circulation modeling, in *Climate System Modeling*, edited by K.E. Trenberth, pp. 371-412, Cambridge Univ. Press, New York, 1992.
- Hellerman, S., and M. Rosenstein, Normal monthly wind stress over the world ocean with error estimates, *J. Phys. Oceanogr.*, 13, 1093-1104, 1983.
- Hirst, A.C., and W. Cai, Sensitivity of a world ocean GCM to changes

- in subsurface mixing parameterization, *J. Phys. Oceanogr.*, **24**, 1256-1279, 1994.
- Hirst, A.C., and T.J. McDougall, Deep water properties and surface buoyancy flux as simulated by a Cartesian model including eddy-induced advection, *J. Phys. Oceanogr.*, **26**, 1320-1343, 1996.
- Hirst, A.C., D. Jackett, and T.J. McDougall, The meridional overturning cells of a world ocean model in neutral surface coordinates, *J. Phys. Oceanogr.*, **26**, 775-791, 1996.
- Levitus, S., Climatological atlas of the world ocean, *NOAA Prof. Pap.* **13**, 173 pp., U.S. Gov. Print. Off., Washington, D. C., 1982.
- McDougall, T.J., and J.A. Church, Pitfalls with the numerical representation of isopycnal and diapycnal mixing, *J. Phys. Oceanogr.*, **16**, 196-199, 1986.
- Manabe, S., R.J. Stouffer, M.J. Spelman, and K. Bryan, Transient responses of a coupled ocean-atmosphere model to gradual changes of atmospheric carbon dioxide, I, Annual mean response, *J. Clim.*, **4**, 785-818, 1991.
- Manabe, S., M.J. Spelman, and R.J. Stouffer, Transient responses of a coupled ocean-atmosphere model to gradual changes of atmospheric carbon dioxide, II, Seasonal response, *J. Clim.*, **5**, 105-126, 1992.
- Molina, M.J., and F.S. Rowland, Stratospheric sink for chlorofluoromethanes: Chlorine atom catalysed destruction of ozone, *Nature*, **249**, 810-812, 1974.
- Pacanowski, R.C., K.W. Dixon, and A. Rosati, The GFDL modular ocean model users guide, version 1.0, *GFDL Ocean Group Tech. Rep.* **2**, 46 pp., Geophys. Fluid Dyn. Lab. Ocean Group, Princeton, N.J., 1991.
- Parkinson, C.L., J.C. Comiso, H.J. Zwally, D.J. Cavalieri, P. Gloersen, and W.J. Campbell, Arctic sea ice, 1973-1976: Satellite passive-microwave observations, *NASA Spec. Publ.*, *NASA SP-489*, 296 pp., 1987.
- Pickart, R.S., N.G. Hogg, and W.M. Smethie, Determining the strength of the Deep Western Boundary Current using the chlorofluoromethane ratio, *J. Phys. Oceanogr.*, **19**, 940-951, 1989.
- Redi, M.H., Oceanic isopycnal mixing by coordinate rotation, *J. Phys. Oceanogr.*, **12**, 1154-1158, 1982.
- Rhein, M., The Deep Western Boundary Current: Tracers and velocities, *Deep Sea Res., Part A*, **41**, 263-281, 1994.
- Rix, N.H., and J. Willebrand, A note on the parameterization of mesoscale eddies as inferred from a high resolution circulation model, *J. Phys. Oceanogr.*, **26**, 2281-2285, 1996.
- Robitaille, D.Y., and A.J. Weaver, Validation of sub-grid scale mixing schemes using CFCs in a global ocean model, *Geophys. Res. Lett.*, **22**, 2917-2920, 1995.
- Schmitz, W.J., On the interbasin-scale thermohaline circulation, *Rev. Geophys.*, **33**, 151-173, 1995.
- Smethie, W.M., Tracing the thermohaline circulation in the western North Atlantic using chlorofluorocarbons, *Prog. Oceanogr.*, **31**, 51-99, 1993.
- Toggweiler, J.R., and B. Samuels, Is the magnitude of the deep outflow from the Atlantic Ocean actually governed by southern hemisphere winds?, in *The Global Carbon Cycle*, edited by M. Heimann, pp. 303-331, Springer-Verlag, New York, 1992.
- Toggweiler, J.R., K. Dixon, and K. Bryan, Simulations of radiocarbon in a coarse-resolution world ocean model, 1, Steady state prebomb distributions, *J. Geophys. Res.*, **94**, 8217-8242, 1989.
- Veronis, G., The role of models in tracer studies, in *Numerical Models of the Ocean Circulation*, pp. 133-146, Nat. Acad. of Sci., Washington, D. C., 1975.
- Visbeck, M., J. Marshall, T. Haine, and M. Spall, On the specification of eddy transfer coefficients in coarse resolution ocean circulation models, *J. Phys. Oceanogr.*, **27**, 381-402, 1997.
- Wallace, D.W.R., and J.R.N. Lazier, Anthropogenic chlorofluoromethanes in newly formed Labrador Sea Water, *Nature*, **332**, 61-63, 1988.
- Wanninkhof, R., Relationship between wind speed and gas exchange over the ocean, *J. Geophys. Res.*, **97**, 7373-7382, 1992.
- Warner, M.J., and R.F. Weiss, Solubilities of chlorofluorocarbons 11 and 12 in water and seawater, *Deep Sea Res., Part A*, **32**, 1485-1497, 1985.
- Weiss, R.F., J.L. Bullister, R.H. Gammon, and M.J. Warner, Atmospheric chlorofluoromethanes in the deep equatorial Atlantic, *Nature*, **314**, 608-610, 1985.

M. H. England, Centre for Environmental Modelling and Prediction, School of Mathematics, University of New South Wales, NSW 2052, Australia. (e-mail: M.England@unsw.edu.au)

G. Holloway, Institute of Ocean Sciences, P.O. Box 6000, Sidney, BC, Canada, V8L-4B2. (e-mail: zounds@ios.bc.ca)

(Received October 13, 1997; revised November 6, 1997; accepted November 6, 1997.)